Entropy Effects on Protein Hinges: The Reaction Catalyzed by Triosephosphate Isomerase†

Jingyi Xiang, Ju-yeon Jung, and Nicole S. Sampson*

Department of Chemistry, State University of New York, Stony Brook, New York 11794-3400

Received April 20, 2004; Revised Manuscript Received July 1, 2004

ABSTRACT: Many proteins utilize segmental motions to catalyze a specific reaction. The Ω loop of triosephosphate isomerase (TIM) is important for preventing the loss of the reactive enediol(ate) intermediate. The loop opens and closes even in the absence of the ligand, and the loop itself does not change conformation during movement. The conformational changes are localized to two hinges at the loop termini. Glycine is never observed in native TIM hinge sequences. In this paper, the hypothesis that limited access to conformational space is a requirement for protein hinges involved in catalysis was tested. The N-terminal hinge was mutated to P166/V167G/W168G (PGG), and the C-terminal hinge was mutated to K174G/T175G/A176G (GGG) in chicken TIM. The single-hinge mutants PGG and GGG had k_{cat} values 200-fold lower than that of the wild type and K_m values 10-fold higher. The k_{cat} of double-hinge mutant P166/V167G/W168G/K174G/T175G/A176G was reduced 2500-fold; the K_m was 10-fold higher. A combination of primary kinetic isotope effect measurements, isothermal calorimetric measurements, and ^{31}P NMR spectroscopic titration with the inhibitor 2-phosphoglycolate revealed that the mutants have a different ligand-binding mode than that of the wild-type enzyme. The predominant conformations of the mutants even in the presence of the inhibitor are loop-open conformations. In conclusion, mutation of the hinge residues to glycine resulted in the sampling of many more hinge conformations with the consequence that the population of the active-closed conformation is reduced. This reduced population results in a reduced catalytic activity.

Proteins catalyze a large variety of reactions. Many utilize conformational changes, such as domain displacement or segmental motion to catalyze a specific reaction (*1*). Thus, the question arises: among all of the possible conformations of a flexible protein molecule, which conformations are most important in terms of catalysis and function and how does the protein control which conformations are populated for proper function?

One common type of conformational change involved in catalysis is the opening and closing of an Ω loop. Ω loops are not independently folding domains but are 10−20 amino acid fragments with a small end-to-end distance (*2*). The loops are attached to the main body of the enzyme and are almost always situated at the protein surface. Displacements of 7−10 Å between the different conformational states of the loops have been observed primarily by X-ray crystal structure analysis (*3*). Typically, the relative populations of the conformational states are altered by the presence or absence of a ligand. Kinetic studies have confirmed that these loops are important in enzyme catalysis. For example, the loop may protect a reactive intermediate from undesired side reactions (*4*) or recruit a catalytic group to the active site (*5*, *6*). There is no primary sequence conservation between loops from unrelated enzymes. However, there is high-sequence conservation among loops from the same enzyme or enzyme family. We sought to understand what is important about the structure of a loop for its catalytic role. That is, how does the structure define the dynamic properties of a loop, and how is the population of the conformational states controlled?

One well-characterized example of a protein with a catalytically important Ω loop is triosephosphate isomerase (TIM).[1] TIM catalyzes the interconversion of dihydroxyacetone phosphate (DHAP) and (*R*)-glyceraldehyde-3-phosphate (GAP) via an enediolate intermediate (Scheme 1). Catalysis by the enzyme does not require any cofactors. In addition, it utilizes an 11 amino acid loop, loop 6 (166−176), to bind and constrain the reaction intermediate.

By X-ray crystallography, the two major conformations of loop 6 that have been observed are the open and the closed

† This work was supported by a grant from the American Chemical Society−Petroleum Research Fund (to N.S.). NMR spectrometers, centrifuges, and a fluorimeter were purchased with support from the NSF (CHE0131146, CHE9808439, and CHE9709164).

* To whom correspondence should be addressed. Telephone: (631) 632-7952. Fax: (631) 632-5731. E-mail: nicole.sampson@stonybrook.edu.

[1] Abbreviations: TIM, triosephosphate isomerase; WT, wild type; DHAP, dihydroxyacetone phosphate; GAP, (*R*)-glyceraldehyde-3-phosphate; PGH, phosphoglycolohydroxamate; 2-PGA, 2-phosphoglycolate; NADH, nicotinamide adenine dinucleotide (reduced form); NAD^+, nicotinamide adenine dinucleotide (oxidized form); GOPDH, α-glycerol-3-phosphate dehydrogenase; GAPDH, glyceraldehyde-3-phosphate dehydrogenase; BHAP, bromohydroxyacetone phosphate; ITC, isothermal titration calorimetry; DTT, dithiothreitol; MG, methylglyoxal; P_i, inorganic phosphate; LB, Luria broth; Tris, tris(hydroxymethyl)aminomethane; DEAE, diethylaminoethyl; TEA, triethanolamine; EDTA, ethylenediaminetetraacetate; PGG, P166/V167G/W168G; GGG, K174G/T175G/A176G; PGG/GGG, P166/V167G/W168G/K174G/T175G/A176G.

10.1021/bi049208d CCC: $27.50
Published on Web 08/17/2004

Scheme 1

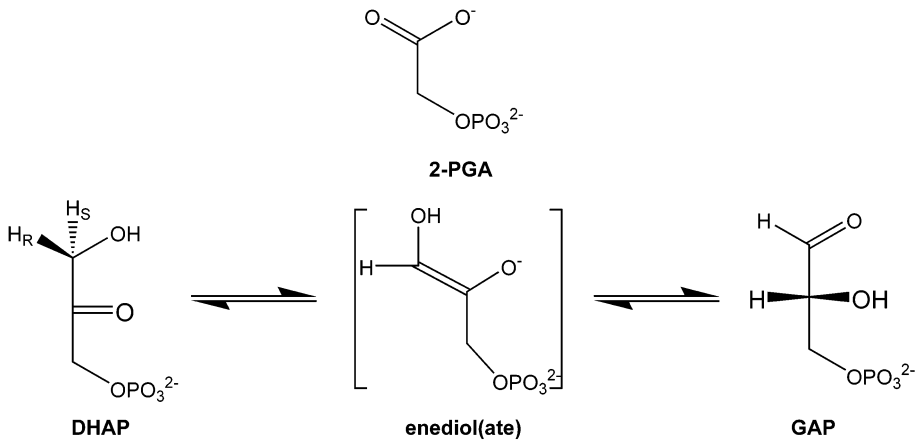

forms (Figure 1). The displacement of the tip of the loop (C_α of Thr172) is around 7 Å. The role of the loop and possible mechanisms for the transit between the open and closed forms of the loop have been investigated by mutagenesis and kinetic studies (*7*−*9*) and NMR dynamics studies (*10*−*12*), as well as molecular dynamics simulations (*13*, *14*). The four residues at the tip of the loop are important for stabilizing the enediol(ate) phosphate intermediate as well

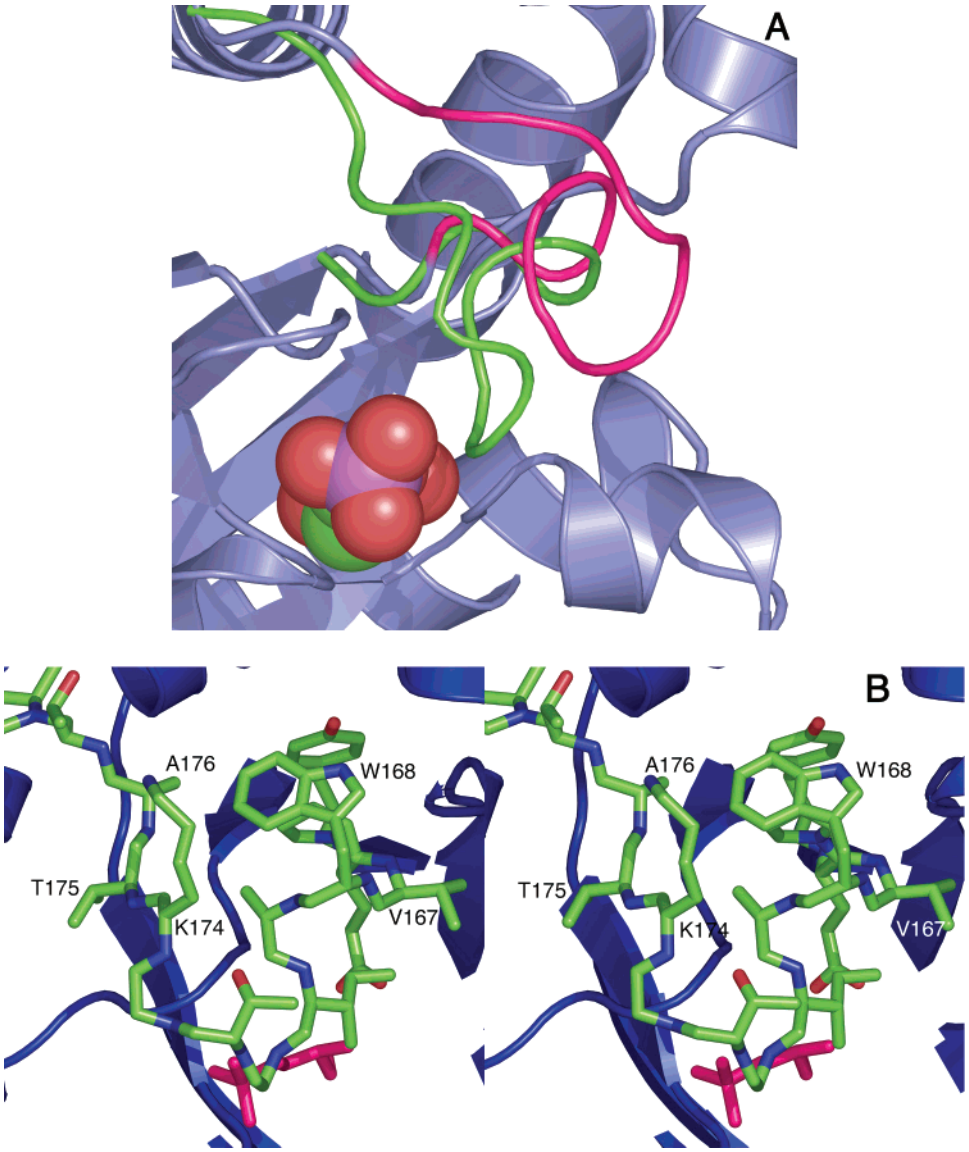

FIGURE 1: (A) Ribbon diagrams depicting the open (magenta) and closed (green) loops of TIM. Glycerol 3-phosphate, a substrate analogue, is shown as a CPK model. (B) Stereorepresentation of the closed loop. Only the side chains of the mutated hinge residues are shown. Glycerol 3-phosphate is shown in magenta. This figure was made using PyMol (*16*) and the PDB 6TIM structure (*17*).

as favoring intermediate protonation over elimination into methylglyoxal and inorganic phosphate (P_i). A hydrogen bond between the hydroxyl of Tyr208 and the amide-NH of Ala176 is required for stabilization and rapid closure of the lid. Structural analysis shows that the transition between these two forms is a rigid "lid" motion and that the loop pivots around 2 hinges, residues 166−168 (N-terminal hinge) and residues 174−176 (C-terminal hinge) (*13*, *15*). Another protein dynamics study provided insight into the time scale of loop motion and suggested that the conformational change of active-site loop 6 may be the rate-limiting step for the enzyme-catalyzed reaction (*14*). Using solid-state deuterium NMR (*10*) as well as ^{19}F solution NMR (*11*), it has been shown that the exchange rate between two states of the labeled Trp168 indole ring on the loop is about 10^4 s^{-1}. This rate is very close to the turnover rate of the enzyme. This observation leads to the suggestion that the conformational change can be the diffusion-controlled rate-limiting step in the enzyme-catalyzed reaction. More interestingly, the exchange rates for the free enzyme and the enzyme with a transition-state analogue, PGH, bound are very similar. These observations suggest that the rate of loop motion is not ligand-gated (*11*). Thus, the enzyme itself may control the rate of loop opening and closing without contributions from ligand binding. Moreover, the hinge region may be the important part of the enzyme that controls loop motion.

The hinges were identified by the comparison of the changes in the ϕ and φ angles of the main-chain backbone between the open and closed forms (*13*). Among the TIMs in different species, the five amino acids comprising the lid of the loop are strictly conserved. The sequence identity of the hinges is strongly conserved, except for Archaebacteria that have compensating sequence changes in loop 7 (*18*). To explore the role of the hinges, we explored the amino acid requirements for the N- and C-terminal hinges as well as the interdependence of sequences for both hinges (*19*, *20*).

Analyzing the amino acid sequence combinations of N- and C-terminal hinges that are functional, we found that the primary constraints are due to sterics (van der Waals interactions) and hydrogen bonds between the hinge residues and the main body of the protein. However, many more amino acid combinations functioned as catalytically competent hinges than are found in nature. These results indicated that the dynamics of the hinges and thus the enzymatic activity may be controlled more by backbone conformational flexibility than by the specific choice of amino acid side chains.

To determine whether the hinge motion and catalysis is dictated by protein backbone flexibility, we constructed glycine-rich hinge mutants in which the side chains of all of the hinge residues except Pro166 were removed. Analysis of interactions between the ligand and hinge residues indicated that there are no direct interactions between the hinge residues and ligand (Figure 2). The ligand makes contact with the lid itself as well as the rest of the protein. We reasoned that mutation of the hinges to glycine should alter the conformational space that may be occupied by the loop without affecting potential ligand-binding interactions. It was unclear whether increasing the number of conformations accessible by the loop would result in reduced diffusion of the substrate into the active site or lower the efficiency of the enolization step. We examined the catalytic profiles

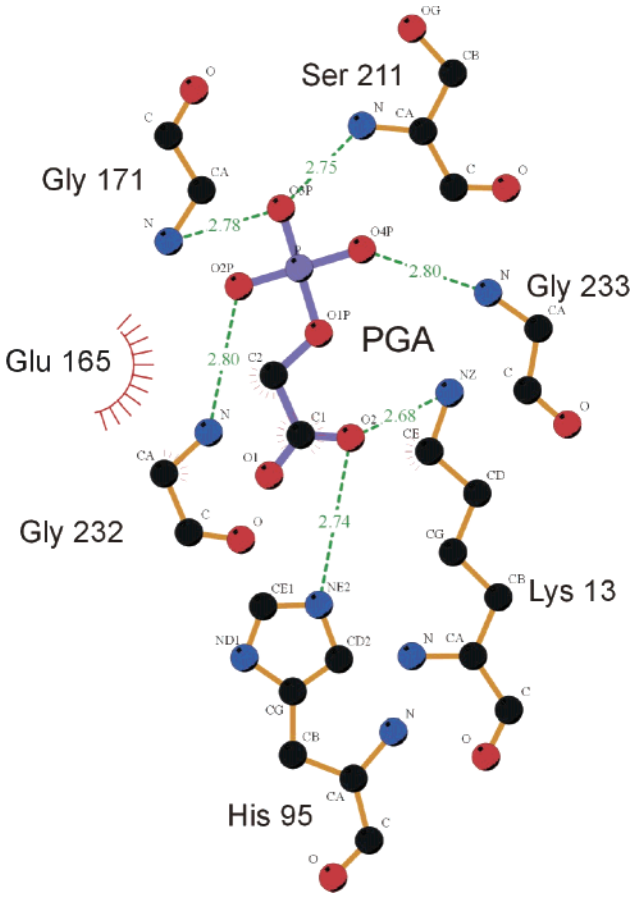

FIGURE 2: Protein contacts with intermediate analogue 2-PGA as determined by Ligplot (*21*). The 0.83 Å resolution structure of *Leishamania mexicana* TIM, PDB 1N55, was used (*22*).

of the N-terminal P166/V167G/W168G (PGG) hinge mutant, the C-terminal K174G/T175G/A176G (GGG) hinge mutant, and the double-hinge P166/V167G/W168G/K174G/T175G/A176G (PGG/GGG) mutant and the thermodynamics of ligand binding. A comparison of the properties of these mutants with those of the wild type (WT) revealed the importance of the hinges in limiting the number of different conformational states that may be populated by limiting conformational flexibility.

EXPERIMENTAL PROCEDURES

Materials. Unless specifically mentioned, all commercial chemicals were used as obtained without further purification, and all solvents were dried and distilled by standard methods prior to use. NADH, DL-glyceraldehyde-3-phosphate (diethyl acetal, monobarium salt), and EDTA were purchased from Sigma Chemical Co. (St. Louis, MO). Aldolase, GOPDH, and GAPDH were obtained from Roche Diagnostics (Indianapolis, IN). For DNA sequencing, the ABI PRISM dye terminator cycle sequencing kit with AmpliTaq DNA PolymeraseFS from Perkin−Elmer (Foster City, CA) was used according to the instructions of the manufacturer. Restriction endonucleases, alkaline phosphatase, T4 polynucleotide kinase, and T4 DNA ligase were from New England Biolabs (Beverly, MA). All other reagents were purchased from Fisher Scientific, Inc. (Springfield, NJ). Oligonucleotide primers were ordered from Integrated DNA Technologies Inc. (Coralville, CA). Their sequences are as follows. Primer 1, 5′-GAGCTGTTGACAATTAATCATCCGGCTCG-3′;

primer 2, 5′-GAGTAGCAGTTTTACGGTTCCGATAG-CACCACCTGGCTCATAGGCAAGAAC-3′; primer 3, 5′-CTATCGGAACCGGTGGAGGTGGTACTCCCCAACAGG-CTCAGGAGGTTCATGAGAAGC-3′; and primer 4, 5′-CCATTCGCCATTCAGGCTGCGCAACTG-3′.

Escherichia coli strain XL1Blue (tet^R) was used for plasmid construction. *E. coli* strain DF502 ($strep^R$, tpi^-, and his^-) used for protein expression was from Drs. D. Fraenkel and J. R. Knowles and has been described previously (*23*). The plasmid pBSX1cTIM (WT) was from Drs. E. Komives and J. R. Knowles (*24*). The construction of pTM03 plasmid has been described previously (*19*).

Construction of PGG, GGG, and PGG/GGG Hinge Mutants. Mutations were introduced by PCR cassette mutagenesis. N-terminal hinge mutant PGG (PVW in WT sequence 166−168) was constructed using primers 1 and 2. An antisense primer, which had the desired codon change to V167G/W168G and included an *Age* I site was used with a sense primer, which complemented the sequence upstream of the TIM gene including an *Nco* I site at the 5′ end of the gene. The resulting PCR fragment was purified and restriction-digested with *Nco* I and *Age* I restriction endonucleases to give a 0.5-kb insert. The pTM03 WT plasmid (*19*) was restricted with the same enzymes and dephosphorylated with alkaline phosphatase, and the 5.8-kb fragment was purified. Using T4 DNA ligase, the insert and vector were ligated to generate pTM11, which encodes the PGG at the N-terminal hinge.

The C-terminal hinge mutant GGG was constructed analogously using primers 3 and 4 and the restriction endonucleases *Age* I and a *Pst* I site at the 3′ end of the gene to generate pTM12.

By subcloning the *Age* I to *Pst* I fragment from pTM12 into pTM11, pTM14 was constructed to provide the PGG/GGG mutant. To increase the protein expression level, the resulting plasmids were further subcloned into pBSX1cTIM vectors as described previously (*20*). The sequences of the constructed mutants were confirmed by DNA sequencing.

Purification of Mutant TIM. Cell paste (∼20 g) of DF502 (pBSX1cTIM) (PGG, GGG, and PGG/GGG) obtained from LB/amp/strep medium (2 L) grown for 24 h was suspended in buffer (10 mM Tris-HCl, 1 mM EDTA at pH 7.6 and 25 °C), and then lysed by two passages through a French press at 10 000 psi and 4 °C. Cell debris was removed by ultracentrifugation at 200000*g* for 90 min. All subsequent purification steps were conducted at 4 °C. The supernatant was loaded onto a column (150 mL) of DEAE cellulose (DE-52, Whatman) pre-equilibrated with buffer (10 mM Tris-HCl at pH 7.5), and the protein was eluted with a linear gradient (0−200 mM, 200 + 200 mL) of KCl in buffer (10 mM Tris-HCl at pH 7.5). Fractions were collected and analyzed by SDS−PAGE. Fractions greater than 95% pure were collected, pooled, and desalted using an Amicon concentrator (YM10 10 000 MWCO, Amicon, Danvers, MA). The sample was loaded onto a second DE-52 column and eluted with a linear gradient (0−200 mM, 200 + 200 mL) of KCl in buffer (10 mM Tris-HCl at pH 6.5). If needed, the protein was purified once more on a Mono Q 5/5 column in buffer (10 mM Tris-HCl at pH 7.5) and eluted using a KCl gradient (0−120 mM, 50 + 50 mL). Fractions containing the mutant were pooled, concentrated, and desalted by Amicon into buffer (10 mM Tris-HCl at pH 7.5). The amount of total protein was determined by a Bradford assay (*25*) using WT chicken TIM as a standard.

Enzyme Assays. TIM activity for WT and mutant TIMs was measured following a modified protocol of Plaut and Knowles (*26*). A total of 1 unit of isomerase activity is the amount of enzyme required to convert 1 μmol of GAP to product in 1 min at 30 °C. With GAP as the substrate, the assay mixture was comprised of NADH (0.35 mM), GOPDH (0.017 mg/mL), and GAP (0.016−10.0 mM), in 1 mL of buffer (100 mM triethanolamine-HCl and 10 mM EDTA at pH 7.6). With DHAP as the substrate, the assay mixture was comprised of NAD^+ (0.35 mM), sodium arsenate (10 mM), GAPDH (0.17 mg/mL), and DHAP (0.016−10 mM), in 1 mL of buffer (100 mM triethanolamine-HCl and 10 mM EDTA at pH 6.5). Initial rates (the first 10% of the reaction) were measured at each substrate concentration with the appearance or disappearance of NADH at 340 nm. The k_{cat} and K_m for GAP were obtained from nonlinear least-squares analyses of plots of S_0 (initial substrate concentration) versus v_i (initial velocity). The K_i values for arsenate were determined with five different concentrations of GAP and five different concentrations of arsenate, and the data fit simultaneously using GraFit (Erithacus Software, Ltd., U.K.). The K_m for DHAP was calculated from nonlinear least-squares analyses of plots of S_0 versus v_i, taking into account the K_i of arsenate.

Inhibition with 2-PGA. The concentration of a solution of 2-PGA was determined by the colorimetric assay of the inorganic phosphate released by alkaline phosphatase. WT or mutant isomerases were assayed at five different concentrations of GAP in the presence of five different 2-PGA concentrations in 100 mM triethanolamine-HCl and 10 mM EDTA at pH 6.5. The K_i values were determined by simultaneously fitting the data using GraFit to a competitive inhibition model.

UV Spectroscopic Titration of 2-PGA Binding. The binding of 2-PGA to the enzyme was monitored by the changes in absorbance at 282 nm, in 10 mM Tris-HCl at pH 6.5 and 25 °C (*27*). The enzyme concentration was 0.4 mg/mL.

Primary Kinetic Isotope Effect. [1(*R*)-^{2}H]-DHAP was prepared using a modified procedure of Leadlay et al. (*28*). DHAP (40 mg) was equilibrated in 3 mL of D_2O with 50 μg of WT TIM under Ar in a 10-kD Centricon (Amicon, Danvers, MA) and incubated at 37 °C for 2 h. After TIM was removed by ultrafiltration, BHAP treated aldolase (50 μg) was added to the reaction mixture and incubated at 37 °C for another 2 h. Then, the aldolase was removed by ultrafiltration. The resulting mixture of [1(*R*)-^{2}H]-DHAP and fructose 1,6-bisphosphate was dissolved in 100 mL of water and loaded onto a 6 × 10 cm anion exchange column (AG-1-X8 Cl^- pre-equilibrated in HCl at pH 3.8), washed with 20 mL of HCl at pH 3.2, and eluted with 60 mL of HCl at pH 1.7. The absorbance of the eluant was monitored at 220 nm. The DHAP-containing fractions were collected, neutralized with 2 M NaOH, and concentrated by lyophilization. The ^{1}H NMR spectrum showed 90% incorporation of deuterium. Using the synthesized [1(*R*)-^{2}H]-DHAP as a substrate, initial rates were measured as described above. The primary kinetic isotope effect was calculated with GraFit using two parameters, the fraction of isotope, f_i, and the substrate concentration, S_0, and fitted to the combined initial

Table 1: Kinetic Parameters for Mutant and WT TIMs

	$k_{cat,GAP}$ (s^{-1})	$K_{m,GAP}$ (mM)	$k_{cat,DHAP}$ (s^{-1})	$K_{m,DHAP}$ (mM)	$K_{i,arsenate}$ (mM)
WT[a]	4300	0.47	430	0.97	11
NPN[b]	5200 ± 110	1.6 ± 0.1	620 ± 17	5.0 ± 0.2	25 ± 1
PGG	240 ± 10	1.2 ± 0.1	50 ± 2	11 ± 4	30 ± 2
GGG	261 ± 13	3.7 ± 0.3	54 ± 4	15 ± 3	29 ± 2
PGG/GGG	1.7 ± 0.1	4.0 ± 0.3	0.25 ± 0.02	18 ± 5	31 ± 2

[a] See ref *30*. [b] See ref *7*.

velocity v_i data sets for [1(*R*)-^{2}H]-DHAP and [1(*R*)-^{1}H]-DHAP.

Methylglyoxal Formation. Methylglyoxal formation was monitored at a single substrate concentration using the method of Richard (*29*). The enzyme concentration was 30 μM, and the [^{32}P]DHAP concentration was 0.15 nM. Time points were collected over 20 h.

^{31}P NMR Spectroscopy. Fourier transform ^{31}P NMR spectra were acquired at 101.3 MHz on a Bruker AC-250 superconducting spectrometer. Sample volumes of 0.6−1.0 mL in a 5-mm diameter NMR tube were used. A total of 15% D_2O was included for frequency locking. All spectra were recorded with broad-band proton decoupling at 250 MHz. Generally, ^{31}P NMR spectra were measured with a 7000-Hz width and 33 000 data points. An acquisition time of 4.7 s and a pulse delay of 1 s were utilized. Line broadening of 2 Hz was applied to the time domain data using 33 000 points. ^{31}P chemical shifts were referenced to external 85% phosphoric acid at 0 ppm at 25 °C.

Isothermal Titration Calorimetry (ITC). ITC experiments were performed using model MCS instruments from MicroCal, Inc. (Northampton, MA). Injections of 10 μL of 2-PGA solution (1.0−2.5 mM in 10 mM Tris-HCl at pH 6.5) were added into the sample solution of TIM (cell volume = 1.483 mL) with stirring at 300 rpm at 30 °C. Control experiments performed by making identical injections of 2-PGA into a cell containing buffer without protein showed insignificant heat of dilution. The concentrations of the WT and mutant TIMs were 100−500 μM. Titrations were carried out in 10 mM Tris-HCl buffer at pH 6.5 and 30 °C. The experimental data were fitted to a one-site binding model using software supplied by MicroCal, Inc., with ΔH (enthalpy change in kcal/mol), K_a (association constant in M^{-1}), and N (number of binding sites per active site) as adjustable parameters. Thermodynamic parameters were calculated from the equation

$$\Delta G = \Delta H - T\Delta S = -RT \ln K_a \qquad (1)$$

where ΔG, ΔH, and ΔS are the changes in free energy, enthalpy, and entropy of binding, T is the absolute temperature, and $R = 1.98$ cal mol^{-1} K^{-1}.

RESULTS

Construction and Expression of Glycine-Rich Hinge Mutants. To investigate the role of the side chains of the N- and C-terminal hinge residues, three glycine-rich TIM hinge mutants were constructed. Five of the six hinge amino acids were mutated to glycine. The proline residue at position 166 was retained because previous work had demonstrated that this proline is critical for TIM activity (*20*). The N-terminal hinge mutant PGG, C-terminal hinge mutant GGG, and the double-hinge mutant PGG/GGG were constructed. Circular dichroism spectroscopy showed that the secondary structure of each of the mutants was identical to that of the WT (data not shown).

Table 2: Inhibition Constant K_i (2-PGA) for Mutant and WT TIMs

enzyme	K_i (μM)[a]	enzyme	K_i (μM)[a]
WT[b]	21 ± 4	GGG	218 ± 10
PGG	170 ± 11	PGG/GGG	260 ± 19 (220 ± 7)[c]

[a] Determined using GAP as a substrate. [b] See ref *31*. [c] Determined by UV at 282 nm.

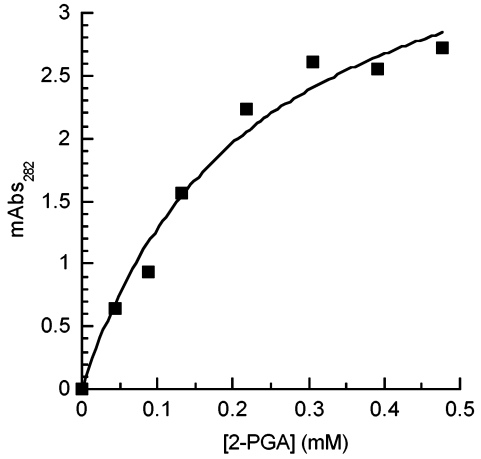

FIGURE 3: UV spectroscopic titration of PGG/GGG mutant TIM (0.40 mg/mL) with 2-PGA at 282 nm in 100 mM triethanolamine-HCl and 10 mM EDTA buffer at pH 6.5 and 25 °C.

Steady-State Kinetics. The steady-state kinetic parameters for the WT and mutant TIMs were determined in both the forward (DHAP → GAP) and the reverse (GAP → DHAP) directions (Table 1). The k_{cat} for PGG/GGG in both directions dropped more than 2500-fold lower than that of the WT, whereas the k_{cat} values for the PGG and GGG mutants dropped approximately 200-fold. The K_m values for the PGG, GGG, and PGG/GGG mutants all increased 4−10-fold.

Inhibition by 2-PGA. To further explore the effect of the loop side-chain deletion on ligand binding, inhibition by 2-PGA, an intermediate analogue, was assayed using GAP as a substrate (Scheme 1). All three mutants showed 10-fold increases in K_i that is weaker binding of the analogue (Table 2). The pattern of inhibition was competitive. We confirmed that 2-PGA is binding to PGG/GGG by monitoring changes in the tyrosine extinction coefficient at 282 nm (Figure 3). The K_d determined from our spectroscopic titration matched the K_i determined kinetically.

Methylglyoxal Formation. The side reaction that results from decomposition of the enediol(ate) intermediate generates the byproducts, methylglyoxal and P_i. The rate of P_i

Table 3: Primary Isotope Effects on WT and Mutant Enzymes

enzyme	$^{D}(V/K)^{a}$	enzyme	$^{D}(V/K)^{a}$
WT[b]	3.6	GGG	2.7 ± 0.1
NPN[b]	3.0 ± 0.1	PGG/GGG	2.6 ± 0.1
PGG	2.6 ± 0.1		

[a] Assayed using [1(*R*)-^{2}H]-DHAP. $^{D}(V)$ is the same as $^{D}(V/K)$. [b] Values reported in ref *32*.

Table 4: Thermodynamic Parameters Determined for the Binding of 2-PGA to TIMs[a]

	ΔH (kcal mol^{-1})	ΔS (cal mol^{-1} K^{-1})	ΔG (kcal mol^{-1})	K_D (μM)
WT	−8.2	−3.7	−7.0	8.4
NPN	−6.2	−0.87	−6.0	51
GGG[b]	∼0	16.9	−5.1	198
PGG/GGG[b]	∼0	16.4	−5.0	260
PGG	−2.0	10.7	−5.3	152

[a] Concentrations used for protein (100−250 μM) and 2-PGA (1−2.5 mM). [b] No heat was detected in the ITC experiment, calculated from the inhibition results in Table 2.

elimination by the mutants is the same as that measured for the WT, 1.7 ± 0.2 M^{-1} s^{-1}. In other words, the *rate* of the byproduct formation does not increase relative to that of the WT enzyme; however, the *partition ratio* of methylglyoxal/product GAP formation has increased for the mutant enzymes because the rate of GAP production is decreased.

Primary Kinetic Isotope Effects. The primary kinetic isotope effect was measured using [(1*R*)-^{2}H]-DHAP as the substrate for the glycine hinge mutants (Table 3). The PGG, GGG, and PGG/GGG mutants all showed similar primary kinetic isotope effects as that of the WT. Because of the loss of the ^{2}H after enolization, the primary deuterium kinetic isotope effect only reports on the relative kinetic barrier heights up to the formation of the enediol(ate) intermediate. The results indicate that the enolization is the rate-limiting step for all three mutants, just as for the WT enzyme.

ITC. ITC was used to measure the binding energetics of 2-PGA, the intermediate analogue (Table 4). The thermodynamic parameters were determined for the WT, NPN (an active C-terminal hinge mutant) (*32*), PGG, GGG, and PGG/GGG. A typical binding isotherm for the WT is shown in Figure 4. The results are summarized in Table 4. Although the WT and NPN enzymes have different binding constants, they both show a similar pattern of negative enthalpy and negative entropy. For the PGG/GGG and GGG mutants, no evolution of heat was detected upon addition of the ligand even at a high concentration of protein (250 μM).

The K_d determined by ITC for the WT and the NPN mutant is consistent with the kinetic K_i. The data indicated that the tight binding of 2-PGA to the WT comes from a large enthalpy change (−8.2 kcal/mol) during the binding process. The entropy change (−6.0 cal/mol K) is actually unfavorable for binding but is compensated by the enthalpic contribution. The NPN mutant binds the ligand more weakly but follows a trend similar to that of the WT. In contrast, the PGG/GGG and GGG mutants do not show any significant enthalpy change during the binding process. Thus, entropy must favor the binding process, and binding of the ligand to these mutants is entropy-driven. The thermodynamic parameters for the PGG mutant are intermediate between the WT and these mutants.

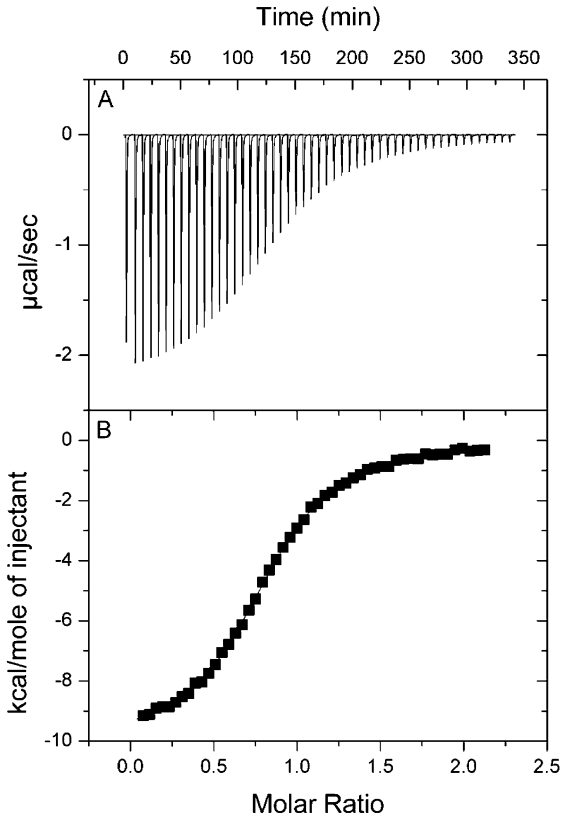

FIGURE 4: Typical ITC curve of TIM + 2-PGA. (A) Raw ITC data output for the interaction between 2-PGA (1 mM) and WT TIM (0.1 mM) at 30 °C and pH 6.5. (B) Titration plot derived from the integrated raw data from A. The line represents the best least-squares fit to the data.

^{31}P NMR of 2-PGA Bound to WT and Mutant TIM. ITC and K_i measurements suggested different binding modes for the glycine-rich hinge mutants versus WT TIM. To explore the difference in the ligand bound form of the enzyme, ^{31}P NMR spectroscopy was used. The ^{31}P nucleus is very sensitive to environmental change, and the changes in the ^{31}P chemical shift of the ligand should reflect changes in the nearby loop and protein structure. The results are presented in Figure 5. All of the spectra were acquired at two different ligand concentrations. An equimolar concentration (to enzyme active sites) of 2-PGA was used to determine the ^{31}P chemical shift for enzyme-bound 2-PGA, whereas a high (4 equiv relative to the enzyme active sites) concentration was used to determine the chemical shift of free 2-PGA and the qualitative exchange rate between these two forms. In the case of the WT, the exchange between free and bound forms is sufficiently slow ($\ll$400 s^{-1}) that peaks corresponding to the two species are observed in the ^{31}P spectrum. As shown in parts a−e of Figure 5, the ^{31}P chemical shifts of ligand bound to the WT and the NPN mutant appear as broad peaks at 5.35 ppm, while the free 2-PGA appears as a sharp peak at 3.25 ppm. The ligand bound to the PGG/GGG and GGG mutants has a chemical shift similar to that of free 2-PGA (parts h−k of Figure 5). The GGG-bound 2-PGA is broadened relative to free 2-PGA, whereas the PGG/GGG-bound 2-PGA has an identical line width to free 2-PGA. Ligand bound to PGG has a chemical shift similar to ligand bound to the WT, although it is significantly broadened (parts f and g of Figure 5). At 4 °C, the line shape did not narrow

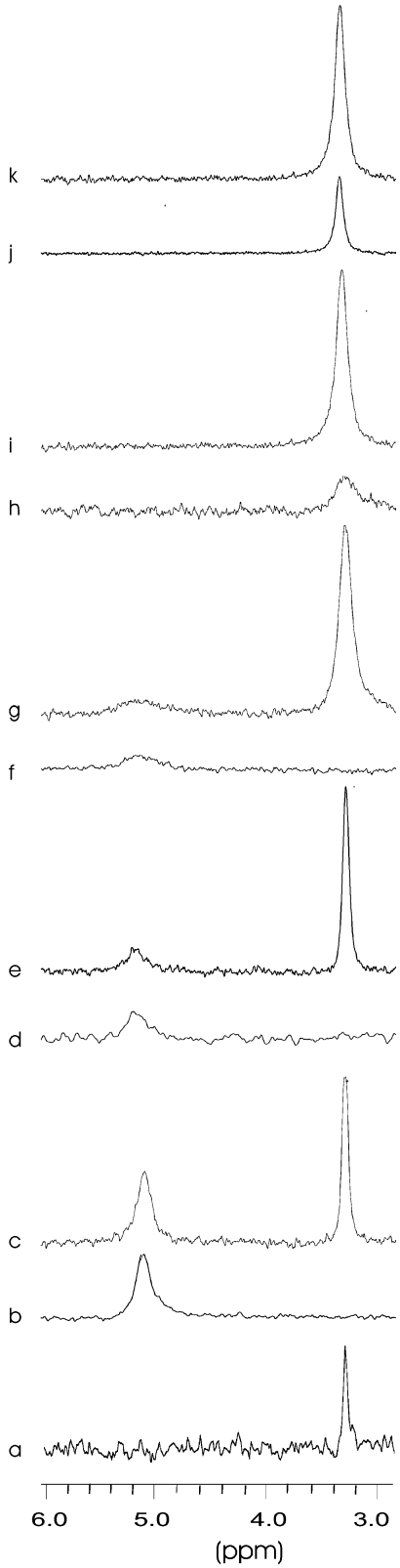

FIGURE 5: ^{31}P NMR spectra of 2-PGA titrations of proteins containing 1 mM TIM (active sites) in 100 mM triethanolamine-HCl and 10 mM EDTA at pH 6.5 and 25 °C. (a) 1 mM 2-PGA; (b) 1 mM WT + 1 mM 2-PGA; (c) 1 mM WT + 4 mM 2-PGA; (d) 1 mM NPN + 1 mM 2-PGA; (e) 1 mM NPN + 4 mM 2-PGA; (f) 1 mM PGG + 1 mM 2-PGA; (g) 1 mM PGG + 4 mM 2-PGA; (h) 1 mM GGG + 1 mM 2-PGA; (i) 1 mM GGG + 4 mM 2-PGA; (j) 1 mM PGG/GGG + 1 mM 2-PGA; and (k) 1 mM PGG/GGG + 4 mM 2-PGA. For each spectrum, the data set contained 6000 transients, except a, which contained 250 transients, and c, which contained 1600 transients. All spectra were acquired at 101.3 MHz.

and the peaks did not shift (data not shown). These results indicate that the phosphate of 2-PGA is bound in an increasingly solvated chemical environment with increasing conformational freedom in the series of mutants PGG, GGG, and PGG/GGG. This increased solvent exposure is in contrast to the N-terminal mutant NPN in which the phosphate chemical environment appears similar to the WT. However, the increased line width of the NPN-bound 2-PGA suggests conformational heterogeneity in this complex as well. This spectrum is consistent with the structural changes observed in the 2-PGA liganded X-ray crystal structure (*18*).

DISCUSSION

In the X-ray crystal structures of TIM, loop 6, which is comprised of 11 amino acids, occupies two distinct conformations depending on the presence of the ligand (*33*, *34*). The superimposition of liganded and unliganded enzymes shows that the loop undergoes a large movement at the loop tip residue Thr172 (Figure 1). The loop structure does not change conformation (*15*). However, residues at the ends of the loop act as hinges. In addition, the peptide bonds between Gly209 and Gly210 and between Gly210 and Ser211 in loop 7 undergo a 90° rotation upon closure. The ϕ/φ bonds of Ser211 rotate from 80°/120° to 65°/30° in the closed form. Our earlier work to investigate the amino acid sequence requirements at the N-terminal (residues 166−168) and C-terminal hinges of loop 6 indicated that specific combinations of amino acids worked best (*19*, *20*, *32*).

To further explore the structure−reactivity relationship between hinge side chains and catalysis, we constructed glycine hinge mutants to test the effect of deletion of hinge side chains. In all of our library selections using growth complementation of the TIM$^-$ strain DF502 (*35*) on glycerol (stringent conditions with a 2-day selection), we had never observed a glycine at multiple hinge positions. We reasoned that replacement of the hinges with glycine would maintain the same peptide backbone constraints as WT TIM throughout the loop but would increase flexibility at the hinges. The first residue of the N-terminal hinge, Pro166, was retained because it is invariant in all known TIM sequences and we knew that it is essential for enzyme catalysis (*20*). Val167 and Trp168 of the N-terminal hinge and Lys174, Val175, and Ala176 of the C-terminal hinge were replaced with two and three glycines, respectively. The resulting N-terminal glycine-rich mutant PGG and C-terminal mutant GGG were combined to construct a glycine-rich double-hinge mutant, PGG/GGG. The three mutant proteins were then purified to homogeneity and characterized with steady-state kinetics. The k_{cat} for the PGG/GGG mutant drops dramatically by 2500-fold in both the forward and reverse direction, while the k_{cat} values of the two single-hinge mutants drop to an intermediate level, around 200-fold. This result is consistent with our previous screening results in which multiple glycines were not observed in the hinges of mutants selected from our libraries. The effects on k_{cat} of the double-hinge mutation were less than additive reflecting the interdependence of hinge residues that had been surmised from earlier mutation selection experiments (*20*) and confirmed by X-ray crystallography of the mutants (*18*). On the other hand, the K_m values were increased by approximately 10-fold for all of the mutants. The values of K_i for the intermediate analogue 2-PGA were increased by a similar amount.

Having shown that the deletion of loop side chains has a dramatic effect on catalysis, we asked whether the underlying reason for the loss of activity was due to a reduction in the enolization step or in the binding of the substrate. The primary deuterium kinetic isotope effect was determined using [1(*R*)-^{2}H]-DHAP as the substrate. Only the relative heights of the substrate binding and enolization steps are probed with [1(*R*)-^{2}H]-DHAP because the isotope is lost upon formation of the intermediate (*28*). If the deletion of hinge side chains affects mainly the diffusion of the substrate into or product out of the active site and the chemistry step was only marginally affected, there would be no isotope effect observed. For all three mutants, we observed a primary kinetic isotope effect comparable to that of the WT, indicating that the enolization step is still rate limiting. Thus, removal of hinge side chains results in a reduction in the catalyzed rate of the chemical steps, that is, enolization and protonation.

In solution, the enediol(ate) intermediate is prone to phosphate elimination forming methylglyoxal >100-fold faster than the protonation reaction to reform triosephosphate (*29*). In the reaction catalyzed by WT isomerase, isomerization is 10^5-fold favored over phosphate elimination. One proposed role of the loop is to prevent elimination of the enediol(ate) intermediate by constraining the phosphate of the intermediate to be in the plane of the enediol, that is, O3 is not periplanar to the π system of the enediol (*7*). Recent structural studies of the DHAP Michaelis complex call into question this proposal. The structures show that the substrate is not strained in the loop-closed form and suggest that this strain is not introduced into the intermediate (*36*). We find that the absolute turnover number of the glycine hinge mutants to form methylglyoxal is identical to that of the WT isomerase. This result combined with the kinetic data suggests that the most important role of the loop hinges is to lower the activation energy of the enolization steps by allowing loop closure. The stabilization of these transition states must arise from a combination of orienting catalytic groups with respect to the substrate and providing a binding site with a dielectric conductive to enolization. Thus, the role of the loop is to ensure that protonation of the enediol(ate) intermediate is faster than elimination by providing a suitably oriented proton at highly effective concentration. In turn, binding of the substrate stabilizes the loop-closed conformation that is catalytically active.

Calorimetric measurements revealed that binding of the ligand to the WT enzyme was enthalpically favorable and the calculated entropy change was negative. These thermodynamics are consistent with an increase of the active-site order upon binding ligand, despite the release of water that occupies the active site in the absence of the ligand. The negative entropy is compensated by strong noncovalent binding interactions between the ligand and protein. Richard and co-workers have estimated that 4 kcal/mol of binding energy in the ground state is derived from binding the phosphate (*37*). This estimate is consistent with our calorimetric measurements on the intermediate analogue. The only direct contact between a loop residue and the ligand is a hydrogen bond between the phosphate moiety of the ligand and the amide of Gly171 at the tip of the loop. The hinge residues do not directly interact with the ligand.

In the series of glycine mutants, we observed a decrease of enthalpy and an increase of entropy along the series PGG, GGG, and PGG/GGG. GGG and PGG/GGG show no detectable enthalpy change upon binding the ligand even at 250 μM protein concentrations, despite the only 10-fold reduction in binding affinity compared to that of the WT. The consequences of this observation are 2-fold. First, the driving force for binding is the entropy increase of the system. The thermodynamics suggest that the active site is not as organized as the WT, possibly because the mutant loop can sample many more conformations. That is, the predominant ligand-bound protein conformer or conformers has an open loop. Second, strong positive binding interactions are not formed in the ground state. This deficiency implies again that the predominant ligand-bound protein conformers have an open loop and that the frequency of forming a productive loop-closed complex that can catalyze the enolization is reduced, resulting in reduced catalytic efficiency. The most likely reason for this enthalpy loss is the absence of loop−phosphate interactions. Although the phosphate binds to other protein residues not part of the loop, the net positive enthalpy of these interactions must be canceled by the enthalpic penalty of desolvation of the ligand and the active site. The loss of strong positive binding interactions results in a new positive entropic contribution upon binding. We presume this positive ΔS is due to the loss of ordered water upon binding the ligand. In the case of the WT, the positive entropy gain from water release is canceled by formation of a more ordered active site. For the glycine mutants, an ordered ligand complex is not formed. Using the ice/water entropy change as a model for release of ordered water, the lower limit of expected entropy change is 7 cal/(mol K) (*38*). This entropy allows us to estimate for the PGG/GGG mutant that 2−3 waters are released upon ligand binding, consistent with the water structure observed in unliganded TIMs.

We investigated the structure of the ligand-bound mutants using ^{31}P NMR to probe the local environment of the ligand 2-PGA phosphate when bound to the enzyme. The WT enzyme/2-PGA complex and free 2-PGA are in slow exchange and are separated by 1.9 ppm. In the PGG mutant, the bound peak is much broader than that for the WT. For the GGG and PGG/GGG mutants, the chemical shift of the bound peak is the same as that for the free 2-PGA. We confirmed, using UV spectroscopy (Figure 4) to titrate ligand binding, that the PGG/GGG mutant does actually bind 2-PGA. In the ^{31}P NMR spectra, titration with the ligand does not cause a change in chemical shift of the phosphate nor does lowering the temperature by 21 °C. Thus, the chemical environment of the mutant-bound 2-PGA phosphate is the same as that of the free 2-PGA. The NMR spectra are consistent with the entropy-driven binding measured by calorimetry, and we conclude that the predominant conformations of these mutants even in the presence of 2-PGA are loop-open conformations. This conformation is consistent with the 10-fold increases in K_m observed for both substrates. Our data suggest that many more loop-open conformations are possible for the GGG and PGG/GGG mutants than for the WT loop. The calorimetric and spectroscopic data indicate that the C-terminal hinge (mutated to GGG) is more important structurally, than the N-terminal hinge. This role is consistent with structural (*18*), mutational (*9*), and

computational (*14*) studies that indicate the formation of a hydrogen bond between Tyr208 and the amide of Ala176 is critical for closure of the loop.

Using temperature jump equilibrium perturbation and fluorescence spectroscopy, Callender and co-workers have inferred the existence of a loop-open Michaelis complex that is formed before the loop-closed Michaelis complex (*39*). In WT TIM, the closed complex is the most highly populated complex in the presence of ligands and is consequently what is usually observed by X-ray crystallography. We conclude from our experiments that the active-site loop 6 is sampling many more conformations in the glycine mutants, particularly GGG and PGG/GGG, than in the WT. When the closed conformation is sampled, catalysis can occur. The frequency of sampling this conformation is significantly reduced because the probability of finding the conformation has been decreased by glycine mutation at the hinge. The result is that the efficiency of enolization is reduced and is rate-limiting. Binding of the substrate to the active site does not become rate-limiting. The role of the loop hinges is to constrain motion of the loop and restrict the number of conformations that are accessible. This constraint can be accomplished with many amino acid compositions as we have found in our earlier library selections (*19*, *20*, *32*). The number of amino acid sequences that result in maximum catalytic efficiency is controlled by secondary interactions between hinges and between loop 6 and 7 (*17*). These interactions are necessary for forming the ideal closed-loop 6 conformation that orients Glu165 to deprotonate the substrate and protonate the intermediate and provides the appropriate protein dielectric for catalysis.

The introduction of glycine into the active-site loop of *S*-adenosylmethionine synthetase resulted in similar consequences (*4*). *S*-Adenosylmethionine synthetase has an eight-residue loop that closes on the substrates to make a catalytically competent complex. Dynamics measurements have shown that the loop motion is not gated by the ligand (*40*), just as in the case for TIM. On the basis of Arrhenius analysis, the entropic component of the activation energy, $\Delta S^{\ddagger}$, undergoes a negative−positive switch upon substitution of loop residues with glycine with a magnitude similar to the $\Delta\Delta S$ that we observe with TIM. In that system, the body of the loop was mutated to glycine, leading to a presumably more disordered lid. In our paper, we have shown that introducing conformational mobility at the hinges without disturbing intraloop interactions is sufficient to alter the conformer population of the enzyme. The unfavorable entropies that result from limiting conformational mobility are counteracted by favorable enthalpic contributions that result from binding substrates.

REFERENCES

1. Gerstein, M., Lesk, A. M., and Chothia, C. (1994) Structural mechanisms for domain movements in proteins, *Biochemistry 33*, 6739−6749.
2. Leszczynski, J. F., and Rose, G. D. (1986) Loops in globular proteins: A novel category of secondary structure, *Science 234*, 849−855.
3. Gerstein, M., and Krebs, W. (1998) A database of macromolecular motions, *Nucleic Acids Res. 26*, 4280−4290.
4. Taylor, J. C., Takusagawa, F., and Markham, G. D. (2002) The active site loop of *S*-adenosylmethionine synthetase modulates catalytic efficiency, *Biochemistry 41*, 9358−9369.
5. Gulotta, M., Deng, H., Dyer, R. B., and Callender, R. H. (2002) Toward an understanding of the role of dynamics on enzymatic catalysis in lactate dehydrogenase, *Biochemistry 41*, 3353−3363.
6. Deng, H., Zheng, J., Clarke, A., Holbrook, J. J., Callender, R., and Burgner, J. W., II (1994) Source of catalysis in the lactate dehydrogenase system. Ground-state interactions in the enzyme−substrate complex, *Biochemistry 33*, 2297−2305.
7. Pompliano, D. L., Peyman, A., and Knowles, J. R. (1990) Stabilization of a reaction intermediate as a catalytic device: Definition of the functional role of the flexible loop in triosephosphate isomerase, *Biochemistry 29*, 3186−3194.
8. Sampson, N. S., and Knowles, J. R. (1992) Segmental movement: Definition of the structural requirements for loop closure in catalysis by triosephosphate isomerase, *Biochemistry 31*, 8482−8487.
9. Sampson, N. S., and Knowles, J. R. (1992) Segmental motion in catalysis: Investigation of a critical hydrogen bond for loop closure in the reaction of triosephosphate isomerase, *Biochemistry 31*, 8488−8494.
10. Williams, J. C., and McDermott, A. E. (1995) Dynamics of the flexible loop of triosephosphate isomerase: The loop motion is not ligand gated, *Biochemistry 34*, 8309−8319.
11. Rozovsky, S., Jogl, G., Tong, L., and McDermott, A. E. (2001) Solution-state NMR investigations of triosephosphate isomerase active site loop motion: Ligand release in relation to active site loop dynamics, *J. Mol. Biol. 310*, 271−280.
12. Rozovsky, S., and McDermott, A. E. (2001) The time scale of the catalytic loop motion in triosephosphate isomerase, *J. Mol. Biol. 310*, 259−270.
13. Joseph, D., Petsko, G. A., and Karplus, M. (1990) Anatomy of a conformational change: hinged "lid" motion of the triosephosphate isomerase loop, *Science 249*, 1425−1428.
14. Derreumaux, P., and Schlick, T. (1998) The loop opening/closing motion of the enzyme triosephosphate isomerase, *Biophys. J. 74*, 72.
15. Noble, M. E. M., Wierenga, R. K., Lambeir, A.-M., Opperdoes, R. R., Thunnissen, A.-M. W. H., Kalk, K. H., Groendijk, H., and Hol, W. G. J. (1991) The adaptability of the active site of trypanosomal triosephosphate isomerase as observed in the crystal structures of three different complexes, *Proteins: Struct., Funct., Genet. 10*, 50−69.
16. DeLano, W. L. (2002) The PyMOL molecular graphics system, http://www.pymol.org.
17. Noble, M. E. M., Zeelen, J. P., and Wierenga, R. K. (1993) Structures of the "open" and "closed" state of trypansomal triosephosphate isomerase, as observed in a new crystal form: Implications for the reaction mechanism, *Proteins: Struct., Funct., Genet. 16*, 311−326.
18. Kursula, I., Salin, M., Sun, J., Norledge, B., Haapalainen, A., Sampson, N. S., and Wierenga, R. K. (2004) Understanding protein lids: Structural analysis of active hinge mutants in triosephosphate isomerase, *Protein Eng., Des., Select. 17*, 375−382.
19. Sun, J., and Sampson, N. S. (1998) Determination of the amino acid requirements for a protein hinge in triosephosphate isomerase, *Protein Sci. 7*, 1495−1505.
20. Xiang, J., Sun, J., and Sampson, N. S. (2001) The importance of hinge sequence for loop function and catalytic activity in the reaction catalyzed by triosephosphate isomerase, *J. Mol. Biol. 307*, 1103−1112.
21. Wallace, A. C., Laskowski, R. A., and Thornton, J. M. (1995) LIGPLOT: A program to generate schematic diagrams of protein−ligand interactions, *Protein Eng. 8*, 127−134.
22. Kursula, I., and Wierenga, R. K. (2003) Crystal structure of triosephosphate isomerase complexed with 2-phosphoglycolate at 0.83 Å resolution, *J. Biol. Chem. 278*, 9544−9551.
23. Straus, D., and Gilbert, W. (1985) Chicken triosephosphate isomerase complements an *Escherichia coli* deficiency, *Proc. Natl. Acad. Sci. U.S.A. 82*, 2014.
24. Hermes, J. D., Parekh, S. M., Blacklow, S. C., Köster, H., and Knowles, J. R. (1989) A reliable method for random mutagenesis: The generation of mutant libraries using spiked oligodeoxyribonucleotide primers, *Gene 84*, 143.
25. Bradford, M. M. (1976) A rapid and sensitive method for the quantitation of microgram quantities of protein utilizing the principle of protein-dye binding, *Anal. Biochem. 72*, 248−254.
26. Plaut, B., and Knowles, J. R. (1972) pH-Dependence of the triosephosphate isomerase reaction, *Biochem. J. 129*, 311−320.

27. Johnson, L. N., and Wolfenden, R. (1970) Changes in absorption spectrum and crystal structure of triose phosphate isomerase brought about by 2-phosphoglycollate, a potential transition state analogue, *J. Mol. Biol. 47*, 93−100.
28. Leadlay, P. F., Albery, W. J., and Knowles, J. R. (1976) Energetics of triosephosphate isomerase: Deuterium isotope effects in the enzyme-catalyzed reaction, *Biochemistry 15*, 5617−5620.
29. Richard, J. P. (1991) Kinetic parameters for the elimination reaction catalyzed by triosephosphate isomerase and an estimation of the reaction's physiological significance, *Biochemistry 30*, 4581−4585.
30. Putman, S. J., Coulson, A. F. W., Farley, I. R. T., Riddleston, B., and Knowles, J. R. (1972) Specificity and kinetics of triose phosphate isomerase from chicken muscle, *Biochem. J. 129*, 301−310.
31. Wolfenden, R. (1969) Transition state analogues for enzyme catalysis, *Nature 223*, 704−705.
32. Sun, J., and Sampson, N. S. (1999) Understanding protein lids: Kinetic analysis of active hinge mutants in triosephosphate isomerase, *Biochemistry 38*, 11474−11481.
33. Lolis, E., Alber, T., Davenport, R. C., Rose, D., Hartman, F. C., and Petsko, G. A. (1990) Structure of yeast triosephosphate isomerase at 1.9 Å resolution, *Biochemistry 29*, 6609−6618.
34. Lolis, E., and Petsko, G. A. (1990) Crystallographic analysis of the complex between triosephosphate isomerase and 2-phosphoglycolate at 2.5 Å resolution: Implications for catalysis, *Biochemistry 29*, 6619−6625.
35. Fraenkel, D. (1986) Mutants in glucose metabolism, *Annu. Rev. Biochem. 55*, 317−337.
36. Jogl, G., Rozovsky, S., McDermott, A. E., and Tong, L. (2003) Optimal alignment for enzymatic proton transfer: Structure of the Michaelis complex of triosephosphate isomerase at 1.2 Å resolution, *Proc. Natl. Acad. Sci. U.S.A. 100*, 50−55.
37. Amyes, T. L., O'Donoghue, A. C., and Richard, J. P. (2001) Contribution of phosphate intrinsic binding energy to the enzymatic rate acceleration for triosephosphate isomerase, *J. Am. Chem. Soc. 123*, 11325−11326.
38. Dunitz, J. D. (1994) The entropic cost of bound water in crystals and biomolecules, *Science 264*, 670.
39. Desamero, R., Rozovsky, S., Zhadin, N., McDermott, A., and Callender, R. (2003) Active site loop motion in triosephosphate isomerase: T-jump relaxation spectroscopy of thermal activation, *Biochemistry 42*, 2941−2951.
40. Taylor, J. C., and Markham, G. D. (2003) Conformational dynamics of the active site loop of *S*-adenosylmethionine synthetase illuminated by site-directed spin labeling, *Arch Biochem. Biophys. 415*, 164−171.

BI049208D